ICMIEE20-064

Effect of Dynamic Stall on the Flow Characteristics of a Darrieus Wind Turbine Blade at Low Wind Speed: A Numerical Approach

Md. Tanvir Khan[*]*, Sharif Mujahidul Islam, Mohammad Ilias Inam, Abdullah Al-Faruk*
Department of Mechanical Engineering, Khulna University of Engineering & Technology, Khulna-9203, BANGLADESH

ABSTRACT
Increased concern for the environment has led us in search of eco-friendlier energy sources. Wind energy can be an invigorating option in this regard. Vertical axis wind turbines offer a reliable and auspicious solution for the remote areas that are away from the integrated grid systems. These turbines show a very unpredictable nature especially due to the effect of dynamics stall. In this paper, the influence of dynamic stall and blade vortex interaction is investigated on the flow properties around a vertical axis Darrieus wind turbine blade. The blade is constructed of NACA 0015 airfoil profile and operates under a low tip speed ratio at the wind velocity 1 m/s. A two-dimensional CFD analysis is executed in ANSYS Fluent 16.2 using the realizable k-epsilon turbulence model and enhanced wall treatment. Graphical representations of the pressure coefficient, turbulent kinetic energy, skin friction coefficient are discussed for the different azimuthal positions of the turbine blade. The tangential and normal force around the blade is also calculated and variation of the forces for different blade positions is discussed. Moreover, the coefficient of power at different wind velocities is calculated and analyzed. It is observed that the dynamic stall and blade vortex interaction significantly affect the flow properties and forces around the blade, which results in the fluctuation of power generation.

Keywords: Darrieus Wind Turbine, Dynamic Stall, Blade Vortex Interaction, Coefficient of Power, CFD.

1. Introduction

Due to global environmental pollution emergence, trends towards renewable energy, and green power sources such as wind energy is flourishing. Wind power generation is an efficient alternative to relieve the global warming problem for smaller environmental impact and renewable characteristics that contributes to sustainable development. It is one of the economic renewable sources and a desirable as well as an adaptable alternative to conventional energy sources [1]. Hence extensive research efforts have been assigned to improve the technology of electricity generation through wind [2,3]. Among the two types of the wind turbine– HAWT (Horizontal Axis Wind Turbine), and VAWT (vertical axis wind turbine) – the VAWT system is suitable to be established within the densely populated city areas because of low-speed wind, which is suitable for both the drag (Savonius) and lift (Darrieus) VAWT [4].

VAWT shows very complex unsteady aerodynamics [5, 6]. The cyclic motion of the blade creates a large variation in the angle of attack (α) even under uniform inflow conditions: the aerodynamic loading fluctuates which causes Dynamic stall (DS) [7]. DS is a phenomenon entangling a series of flow separations and reattachments occurring on any lifting surface subjected to a rapid unsteady motion [8]. A plethora of researches have been performed on it and is still continuing. Mandal [9] observed the effects of DS and flow curvature on the aerodynamic performance of straight-blade Darrieus wind turbine (DWT) using the cascade model and found a good correlation between the experimental data and calculated values of the instantaneous blade force and the wake velocities. Overall coefficient of power (COP) of high solidity DWT are significantly varying for the low and high tip speed ratio (TSR). Balduzzi [10] carried out a 3D time-accurate Reynolds-averaged Navier-Stokes (RANS) Computational Fluid Dynamics (CFD) analysis of DWT and observed the flow effects and their impact on the energy efficiency of Darrieus rotor blades. Noll [11] found a positive effect of the DS on the power generation of the wind turbine, although the aeroelastic vibrations, noises from the blades and the fatigue of the blade material occur by the unsteady forces of stall vortices [12]. Measuring the unsteady fluid forces acting on the rotating blade, Laneville and Vittecoq [13] observed that the dynamic variations of lift and drag forces become dominant when the TSRs decrease. Brochier et al. [14] and Fujisawa [15] presented the flow fields around DWT in a water tunnel using laser-doppler velocimetry (LDV) and particle image velocimetry (PIV), respectively. The distributions of mean and fluctuating velocities in the wake are found to indicate a local peak due to the DS by measuring the time-averaged flow properties. The unsteady flow around the DWT operating at low TSR results in the generation of two pairs of stall vortices in one cycle of turbine rotation. Although the structure of the stall vortices is roughly independent of the TSRs, the generating angle of these stall vortices and their development are influenced by the TSRs [16]. Paraschivoiu [17] stated that DS poses an obstacle to the greater implementation of VAWT by reducing turbine efficiency and inducing structural vibrations and noise [18]. This study focuses mainly on the influence of DS and blade vortex interaction (BVI) on the flow properties of a DWT blade at low wind speed. BVI is an unsteady phenomenon of three-dimensional nature, that occurs when a rotor blade passes within a close proximity of the shed tip vortices from a previous blade [40]. These phenomena greatly influence the turbine efficiency by disturbing the flow surrounding the blade and creating impulsive noise especially in low wind speed condition. The pressure coefficient, turbulent kinetic energy, and

* Corresponding author. Tel.: +88-01866937512
E-mail address: tanvir.anik2196@gmail.com

skin friction coefficient are graphically presented and the effect of DS and BVI on these properties is analyzed in this article. Moreover, the tangential and normal forces on the turbine blade are analyzed and the COPs for different wind velocities are calculated and discussed.

2. Computational Setup

2.1 Geometry Generation

A NACA 0015 [19] airfoil of chord length C is selected as the turbine blade, which is placed in an annulus shape zone, generated bi-directionally from the surface of the blade as shown in Fig.1. The radii of the inner and outer circles are 0.85C and 1.2C, respectively, and the blade is placed at 1C distance from the center [20]. This zone with the turbine blade is allowed to rotate at a predefined angular velocity. Finally, the computational domain is constructed as a square shape of side distance 25C from the center of the annulus as applied by Mohamed [21]. Overall the computational domain is constructed of the inner stationary zone, rotating zone and outer stationary zone, successively. Before fixing the domain size several domains were tested and domain independence is ensured as shown in Table 1.

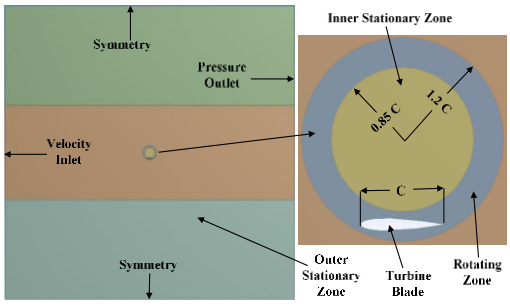

Fig.1 (Left) Boundary conditions in the computational domain, (right) close-up view surrounding the blade.

Table 1 Domain independency test for the analysis

Domain (D)	Inlet/ Wall Distance	Outlet Distance	Upper/ Lower Vertical Wall Distance	% Error
D 1	10C	15C	3C	0.83
D 2	15C	20C	4C	0.018
D 3 [21]	25C	25C	8C	-
D 4	20C	25C	5C	0.01
D 5	15C	25C	6C	0.02

2.2 Mesh Generation

The computational domain is divided into three different rectangular zones to avail optimum mesh and different sizes of unstructured mesh are employed [Table 2]. Element size of 0.003 mm mesh is applied to the inner rectangle in which the rotating zone is posited to precisely analyze the flow properties adjacent to the turbine blade. And element size of 0.008 mm is used the two outer rectangular zones further from the blade to reduce the complexity of grid generation. In the vicinity of the blade surface, 15 inflation layers are used in 5 mm thickness to better resolve the boundary layers Fig.2. The number of inflation layers is selected after the sensitivity analysis as presented in Table 3. This type of combined grid– instead of the single grid only– is also chosen by Qin [6], Hutomo [8], and Bangga [22] and good combination with the experiments were found. Several node and element sizes were taken and the mesh dependency test is performed Fig.3(a). Finally, node 860966 is selected for the analysis.

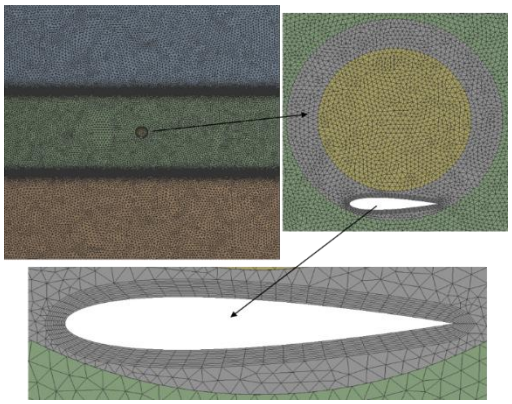

Fig.2 Grid generation and magnifying view around the rotating zone and turbine blade.

Table 2 Number of nodes and elements for the grid independency test [Fig. 3(a)] for the analysis

Mesh	Number of Nodes	Number of Elements
Mesh 1	2471666	4935750
Mesh 2	1232362	2459030
Mesh 3	860966	1919927
Mesh 4	753807	1502883
Mesh 5	525219	1046262

Table 3 Sensitivity of the number of inflation layers near the turbine blade wall

Number of Inflation Layers	Value of Pressure Coefficient	% Error
5	-0.25319	0.228
10	-0.2531	0.011
15	-0.25312	-
20	-0.25308	0.01

2.3 Boundary conditions and solution method

Velocity inlet at the upstream, pressure outlet at the downstream, and no-slip wall at the blade surface are employed as boundary conditions, for performing the simulation while symmetry conditions are used at the other two sides, to reduce the computational effort [23, 24, 25]. The operating pressure is set at 1 atmospheric pressure for the analysis. The blade, located in the rotating zone, can rotate with it at the same predetermined angular velocity as shown in Fig.1. For operating the simulation, clockwise rotation is applied to the turbine blade initially, whereas the air is coming from the inlet at a predefined velocity. As a result of the

combination of air kinetic energy and blade rotation, a net torque is generated on the blade – therefore, lift and drag force has also developed from where the normal and the tangential force has been calculated. The Time step size is taken 0.005 for the analysis after the validation test Fig.3(b). The realizable k-ε turbulence model [3, 26-30] with Enhanced Wall Treatment [31] is used for the rotating zones which has some benefits over the standard k-ε turbulence model stated by Mohamed [21]. All solution variables were solved employing simple pressure-based solver and second-order upwind discretization scheme [22,32].

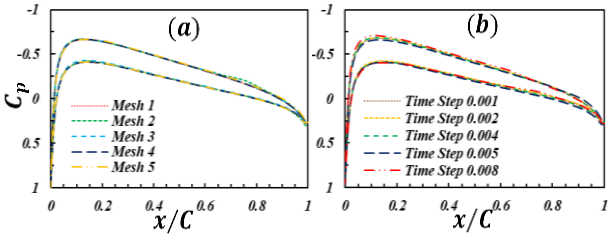

Fig.3 Variation of C_p with chord length around the turbine blade at θ = 1.5° for different (a) node and element numbers,[Table 2] and (b) time step sizes.

3. Result & Discussion

The wind turbine rotation is unsteady at the beginning and after some rotations, it comes to the steady-state condition. So all the simulations were conducted for 10 blade rotations and the average of the last three rotations were considered [22]. The numerical model is validated by comparing the tangential velocity variation with Bangga et al. [22] for the same operating conditions and a good match is found as shown in Fig.4. Pressure coefficient (C_p), turbulent kinetic energy (k), skin friction coefficient (C_f) profiles are presented and analyzed at every 15° interval of azimuthal angle (θ) and the tangential (F_T) force, normal (F_N) force and the COP are calculated.

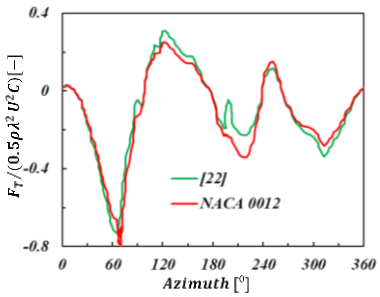

Fig.4 Data validation (Tangential force) for NACA 0012 airfoil shape turbine blade with Bangga et al. [22].

3.1 Effect of DS and BVI on Pressure Coefficient

Pressure coefficient depicts the relative pressure surrounding the flow field– defined by $C_p = \frac{P-P_\infty}{1/2\rho_\infty V_\infty^2}$ [33,34], where P_∞ is the atmospheric pressure. The pressure coefficient is an important factor for wind turbine aerodynamics– causes a significant change in the lift and drag as well as power generation. The effect of DS on C_p along the blade chord length at different blade positions is presented in Fig5. Pressure at the leading edge (LE) of the blade is maximum at θ = 0° [35] and suddenly decreases with the chord length, although near the trailing edge (TE) pressure increases again. When upstream air strikes at the LE, which is the stagnation point, pressure becomes maximum for the high air kinetic energy. Then when air flows over the blade the pressure becomes low, however, at the TE the flow separates and due to boundary layer separation the boundary layer forms a wake– results in an increase in pressure. Moreover, pressure at the blade LE is low at θ = 30°, 45°, 75°, 285°, 300°, 330° and with chord length pressure at blade upper surface is gradually increasing albeit no significant change occurs at blade lower surface. TE pressure is gradually decreasing around the blade chord at θ = 60°, 90°, 150°, 225°, 240°. Furthermore, pressure at the blade upper surface is low till the middle of the blade chord length and then increases towards TE at θ = 120°, 135°, 195°, 210°, 270°, 315°, 345°, however, pressure at the blade lower surface is not varying. Due to the pressure variation around the turbine blade, the tangential and normal forces vary significantly– which greatly influences the turbine power generation [22].

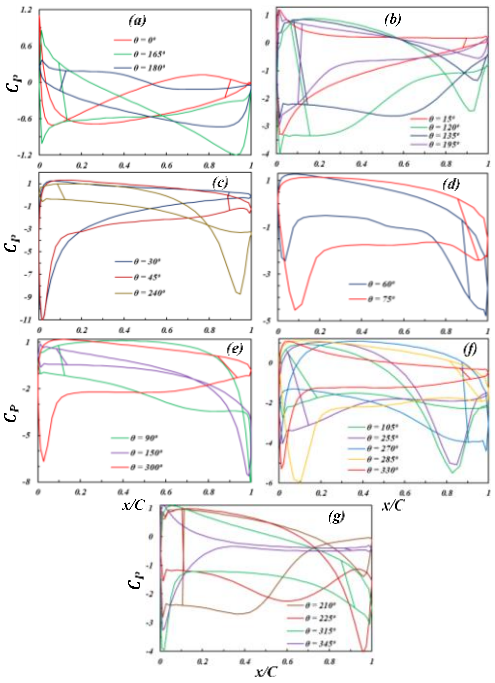

Fig.5 Variation of pressure coefficient around the blade chord length for different azimuthal position of turbine blade.

3.2 Effect of DS and BVI on Turbulent Kinetic Energy

The effect of DS on normalized turbulent Kinetic Energy (k) along the blade chord length at different blade azimuthal position is presented in Fig.6. The normalization is done by $0.5 \times \rho \times U^2$, where, ρ is the

density of air [kg/m^3] and U is the wind velocity [m/s]. Turbulent kinetic energy is significantly affected by the DS and BVI. Turbulent kinetic energy at the blade LE and TE edge are maximum for almost every position of the blade and near the middle of the blade, it's comparatively lower. However, high turbulent kinetic energy is noticed near the middle of the blade at θ = 120°, 135°, 210°, 240°, 270°. Moreover, near the blade TE at θ = 0°, 30°, 45° and near LE at θ = 60°, 135°, 240°, 255° k is found very low. Stall vortices that occur due to DS significantly dominate the turbulent kinetic energy, especially at low TSR.

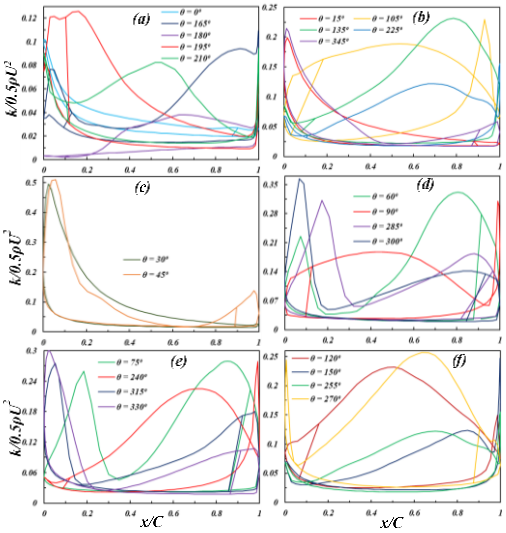

Fig.6 Variation of normalized turbulent kinetic energy around the blade chord length for different blade position.

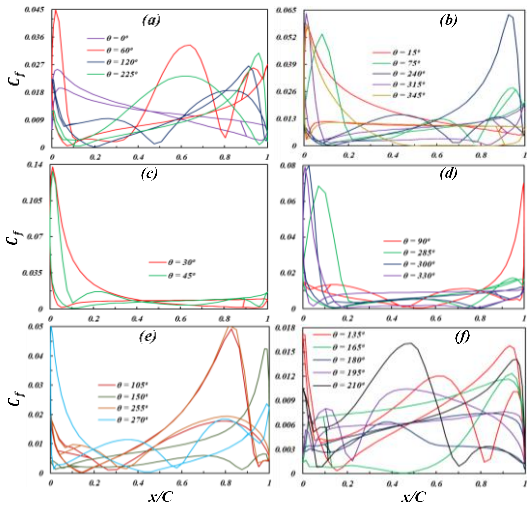

Fig.7 Variation of skin friction coefficient around the blade chord length for different azimuthal position of turbulent blade.

3.3 Effect of DS and BVI on Skin Friction Coefficient

The effect of DS and BVI on skin friction coefficient (C_f) along the blade chord length at different blade positions is presented in Fig.7. Skin friction is significantly influenced by the DS and BVI. C_f at the blade LE is maximum for almost every blade positon. However, at θ = 90°, 105°, 150°, 240°, 255° near the blade TE C_f is observed utmost. Although skin friction at the blade middle is generally low, notwithstanding, it is found high near the middle of the blade at θ = 60°, 135°, 180°, 195°, 225°.

3.4 Effect of DS and BVI on Tangential and Normal Forces around the blade

It is observed from Fig.8 and Fig.9 that both the tangential (F_T) and normal (F_N) forces are greatly influenced by the stall vortex and pressure variation around the turbine blade. To derive the tangential and normal forces– at first the lift and drag forces are calculated from the lift (C_L) and drag (C_D) coefficients. And then the tangential and normal forces are calculated from the lift and drag forces [36]. It is observed that at the beginning of the turbine rotation, both the tangential and normal forces are positive. When the blade comes to θ=45° azimuthal position, pressure at the blade upper surface becomes low and the direction of F_T changes along with the change of C_L and C_D as illustrated in Fig. 8. When the stall vortex separates from the blade upper surface, it tends to increase at θ = 60° until lower pressure occurs at the blade upper surface again as a consequence of DS. For the occurrence of lower pressure at the downstream and high-pressure drag at the blade upstream at θ = 90°, the tangential force decreases gradually. At the blade's position of θ = 120°, stall vortex detached from the blade upper surface, therefore, the force tends to increase.

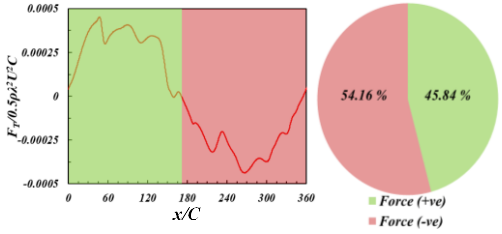

Fig.8 Normalized tangential force along the azimuthal position of turbine blade. It is noted that the negative tangential force generates the positive power.

Different types of vortex form around the blade at θ = 150° and due to the BVI, F_T decreases to θ = 210°. Then the stall vortex tends to come to the middle of the blade and F_T increases. When vortex separates at θ = 240° the force tends to decrease. Tangential force increases at θ = 270°, for higher pressure occurs at the blade upstream zone. Again, low pressure occurs at the TE of the blade at θ = 300°, and the force increases. So, it can be settled conclusively that– for the second half of the blade rotation when the lower pressure occurs at the TE, the tangential force tends to increase. It is determined that the force is positive for the first half cycle (45.84%) and negative for the rest half cycle

(54.16%). Moreover, it is noted that the negative tangential force generates positive power.

The normal force changes dramatically adjacent to the blade surface for the pressure discontinuity [37]. The force grows larger till the blade comes to θ = 45°, then it tends to decay up to θ = 135°, and again proliferates until θ = 190°. After that, the force derogates till θ = 225° and then again rises up until the blade comes to θ = 315°. Again the force drops till θ = 360° and then repeats as shown in Fig.9. It is observed that F_N is positive for 51.95% of blade rotation and negative for 48.05% of the blade rotation.

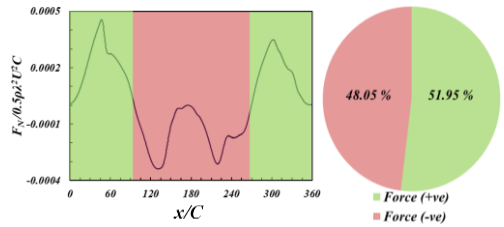

Fig.9 Normalized normal force along the azimuthal position of turbine blade.

3.5 Coefficient of Power for different wind velocities

Coefficient of power (COP) – the most important parameter in the case of power regulation [38] – is defined as the ratio of the turbine output power (P) to the input power (P_{in})[23]. As the turbine rotates clockwise direction the negative tangential force (F_T) generates the positive power which can be defined as $P = -\omega R F_T$ [22] and vice versa. The theoretical input power is $P_{in} = \frac{1}{2}\rho A V^3$[39], where, ρ is the air density [kg/m^3], A is the swept area [m^2] and V is the wind velocity [m/s]. It is clearly observed from Fig.10 that, COP is gradually increasing with the wind velocity and for higher wind velocities the increment of COP is comparatively smaller than the low wind velocities.

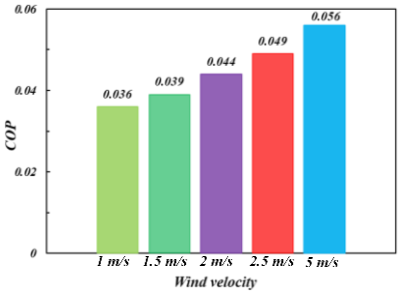

Fig.10 Average coefficient of power at several wind speeds.

4. Conclusion

Numerical analysis has been conducted to study a DWT blade under the DS condition at wind velocities 1 m/s at low TSR. The studied turbine blade is shaped of NACA 0015 airfoil. The flow characteristics encompassing the blade surface are scrutinized and emphasized as the pith of the article. The pressure coefficient, turbulent kinetic energy, skin friction coefficient profile is presented graphically and the effect of DS and BVI on these are discussed. The tangential and the normal force and the average coefficient of power have been calculated. It is observed that for certain azimuthal angles the tangential and normal forces are positively and negatively varying which is directly connected to the wind turbine power generation. Moreover, parameters such as the pressure coefficient, turbulent kinetic energy, skin friction coefficient show a highly unpredictable nature due to the strong influence of the DS and BVI. As these fluctuations are directly connected with the wind turbine performance, consequently, the turbine power generation is also varying abruptly. However, the net power generated by the turbine is positive and the average coefficient of power of the turbine is gradually increasing with the wind velocities.

Nomenclature

C_p : Pressure Coefficient
C_f : Skin Friction Coefficient
F_T : Tangential Force, N
F_N : Normal Force, N
C_L : Lift Coefficient
C_D : Drag Coefficient

References

[1] Miyara, Flow dynamics and heat transfer of wavy condensate film, *Journal of Heat Transfer, Trans. of ASME*, Vol. 123, pp 492-500 (2001).

[2] Bhutta, M. M. A., Hayat, N., Farooq, A. U., Ali, Z., Jamil, S. R., & Hussain, Z. (2012). Vertical axis wind turbine–A review of various configurations and design techniques. *Renewable and Sustainable Energy Reviews*, *16*(4), 1926-1939.

[3] Mohamed, M. H., Janiga, G., Pap, E., & Thévenin, D. (2011). Optimal blade shape of a modified Savonius turbine using an obstacle shielding the returning blade. Energy Conversion and Management, 52(1), 236-242.

[4] Mohamed, M. H. (2013). Impacts of solidity and hybrid system in small wind turbines performance. *Energy*, *57*, 495-504.

[5] Svorcan, J., Stupar, S., Komarov, D., Peković, O., & Kostić, I. (2013). Aerodynamic design and analysis of a small-scale vertical axis wind turbine. *Journal of Mechanical Science and Technology*, *27*(8), 2367-2373.

[6] Qin, N., Howell, R., Durrani, N., Hamada, K., & Smith, T. (2011). Unsteady flow simulation and dynamic stall behaviour of vertical axis wind turbine blades. *Wind Engineering*, *35*(4), 511-527.

[7] Scheurich, F., Fletcher, T. M., & Brown, R. E. (2011). Simulating the aerodynamic performance and wake dynamics of a vertical-axis wind turbine. *Wind Energy*, *14*(2), 159-177.

[8] Hutomo, G. P., Bangga, G. S., & Sasongko, H. (2016). CFD studies of the dynamic stall characteristics on a rotating airfoil. In *Applied Mechanics and Materials* (Vol. 836, pp. 109-114). Trans Tech Publications Ltd.

[9] Mandal, A. C., & Burton, J. D. (1994). The effects of dynamic stall and flow curvature on the aerodynamics of darrieus turbines applying the cascade model. *Wind Engineering*, 267-282.

[10] Balduzzi, F., Drofelnik, J., Bianchini, A., Ferrara, G.,

Ferrari, L., & Campobasso, M. S. (2017). Darrieus wind turbine blade unsteady aerodynamics: a three-dimensional Navier-Stokes CFD assessment. *Energy*, *128*, 550-563.

[11] Noll, R. B., & Ham, N. D. (1982). Effects of dynamic stall on SWECS.

[12] Abramovich, H. (1987). Vertical axis wind turbines: A survey and bibliography. *Wind Engineering*, *11*(6), 334-343.

[13] Laneville, A., & Vittecoq, P. (1986). Dynamic stall: the case of the vertical axis wind turbine.

[14] Brochier, G., Fraunie, P., Beguier, C., & Paraschivoiu, I. (1986). Water channel experiments of dynamic stall on Darrieus wind turbine blades. *Journal of Propulsion and Power*, *2*(5), 445-449.

[15] Fujisawa, N., & Takeuchi, M. (1999). Flow visualization and PIV measurement of flow field around a Darrieus rotor in dynamic stall. *Journal of Visualization*, *1*(4), 379-386.

[16] Fujisawa, N., & Shibuya, S. (2001). Observations of dynamic stall on Darrieus wind turbine blades. *Journal of Wind Engineering and Industrial Aerodynamics*, *89*(2), 201-214.

[17] Paraschivoiu, I., & Allet, A. (1988). Aerodynamic analysis of the Darrieus wind turbines including dynamic-stall effects. *Journal of Propulsion and Power*, *4*(5), 472-477.

[18] Buchner, A. J., Soria, J., Honnery, D., & Smits, A. J. (2018). Dynamic stall in vertical axis wind turbines: scaling and topological considerations. *Journal of Fluid Mechanics*, *841*, 746-766.

[19] El Chazly, N. M. (1993). Static and dynamic analysis of wind turbine blades using the finite element method. *Renewable energy*, *3*(6-7), 705-724.

[20] Khan, M. T., Inam, M. I., & Al-Faruk, A. Numerical Analysis of Flow Characteristics around a Single-bladed Darrieus Wind Turbine. In *International Conference on Energy & Environment (ICEE2018).*

[21] Mohamed, M. H., Ali, A. M., & Hafiz, A. A. (2015). CFD analysis for H-rotor Darrieus turbine as a low speed wind energy converter. *Engineering Science and Technology, an International Journal*, *18*(1), 1-13.

[22] Bangga, G., Hutomo, G., Wiranegara, R., & Sasongko, H. (2017). Numerical study on a single bladed vertical axis wind turbine under dynamic stall. *Journal of Mechanical Science and Technology*, *31*(1), 261-267.

[23] Castelli, M. R., Englaro, A., & Benini, E. (2011). The Darrieus wind turbine: Proposal for a new performance prediction model based on CFD. *Energy*, *36*(8), 4919-4934.

[24] Castelli, M. R., Dal Monte, A., Quaresimin, M., & Benini, E. (2013). Numerical evaluation of aerodynamic and inertial contributions to Darrieus wind turbine blade deformation. *Renewable Energy*, *51*, 101-112.

[25] Raciti Castelli, M., Ardizzon, G., Battisti, L., Benini, E., & Pavesi, G. (2010, November). Modeling strategy and numerical validation for a Darrieus vertical axis micro-wind turbine. In *ASME 2010 international mechanical engineering congress and exposition* (pp. 409-418). American Society of Mechanical Engineers Digital Collection.

[26] Mohamed, M. H., Janiga, G., Pap, E., & Thévenin, D. (2010). Optimization of Savonius turbines using an obstacle shielding the returning blade. *Renewable Energy*, *35*(11), 2618-2626.

[27] Mohamed, M. H., Janiga, G., Pap, E., & Thévenin, D. (2011). Multi-objective optimization of the airfoil shape of Wells turbine used for wave energy conversion. *Energy*, *36*(1), 438-446.

[28] Mohamed, M. H., & Shaaban, S. (2013). Optimization of blade pitch angle of an axial turbine used for wave energy conversion. *Energy*, *56*, 229-239.

[29] Shih, T. H., Liou, W. W., Shabbir, A., Yang, Z., & Zhu, J. (1994). A new k-epsilon eddy viscosity model for high Reynolds number turbulent flows: Model development and validation.

[30] Mohamed, M. H. (2014). Aero-acoustics noise evaluation of H-rotor Darrieus wind turbines. *Energy*, *65*, 596-604.

[31] Liang, Y. B., Zhang, L. X., Li, E. X., & Zhang, F. Y. (2016). Blade pitch control of straight-bladed vertical axis wind turbine. *Journal of Central South University*, *23*(5), 1106-1114.

[32] Khan, M. T., Inam, M. I., & Al-Faruk, A. Effect of Tip Speed Ratio on the Flow Characteristics of Single-bladed Darrieus Wind Turbine. In *International Conference on Mechanical, Industrial and Energy Engineering (ICMIEE2018).*

[33] Costola, D., Blocken, B., & Hensen, J. L. M. (2009). Overview of pressure coefficient data in building energy simulation and airflow network programs. Building and environment, 44(10), 2027-2036.

[34] Zhang, L. X., Liang, Y. B., Liu, X. H., & Guo, J. (2014). Effect of blade pitch angle on aerodynamic performance of straight-bladed vertical axis wind turbine. *Journal of Central South University*, *21*(4), 1417-1427.

[35] Khan, M. T., Inam, M. I., & Al-Faruk, A. (2019, January). CFD Analysis of a Floating Offshore Vertical Axis Wind Turbine. In *International Conference on Sustainability in Natural and Built Environment (iCSNBE2019)* (Vol. 19, p. 22).

[36] Lian, D., Lee, J. H., & Kim, Y. C. (2008). Power prediction of darrieus type wind turbine considering real air velocity on the wind turbine blade. *School of Mech. Eng. Kunsan National Univ.*

[37] Memon, A., Samo, S. R., Asad, M., & Mangi, F. H. (2015). Modeling of Aerodynamic Forces on the Wind Turbine Blades. *Journal of Clean Energy Technologies*, *3*(6).

[38] Rolan, A., Luna, A., Vazquez, G., Aguilar, D., & Azevedo, G. (2009, July). Modeling of a variable speed wind turbine with a permanent magnet synchronous generator. In *2009 IEEE international symposium on industrial electronics* (pp. 734-739). IEEE.

[39] Shamshirband, S., Petković, D., Saboohi, H., Anuar, N. B., Inayat, I., Akib, S., ... & Gani, A. (2014). RETRACTED: Wind turbine power coefficient estimation by soft computing methodologies: Comparative study.

[40] Amet, E., Maître, T., Pellone, C., & Achard, J. L. (2009). 2D numerical simulations of blade-vortex interaction in a Darrieus turbine. Journal of fluids engineering, 131(11).